*The Plymouth Student Scientist, 2017, **10** (2), 40-58*

The effects of turbulence on vertical distributions and concentrations of phytoplankton in (Case II) coastal waters

Daniel Ford

Project Advisor: Jill Schwarz, School of Biological & Marine Sciences, Plymouth University, Drake Circus, Plymouth, PL4 8AA

Abstract

Estuaries are extensive habitats that are vulnerable to rising sea levels; a detailed understanding of biological and physical interactions is required to predict future change. Surveys were conducted in an estuarine system across contrasting tidal states, of neap ebb and spring flood, to evaluate how changes in vertical turbulent mixing affect vertical phytoplankton distributions. Profiles of temperature, salinity, irradiance, shear microstructure and fluorescence were undertaken at multiple stations along the Tamar Estuary, UK. Results confirmed that turbulent mixing was predominately controlled by stratification, with lower mixing occurring on the neap ebb tide. At stations where the average water column mixing was low, chl-a concentrations increased in the surface waters as mixing was not redistributing cells throughout the water column. As mixing increased chl-a concentrations became more homogenous with depth. A decrease was observed in the chlorophyll-a / chlorophyll-b ratio as mixing increased, consistent with photoacclimation of phytoplankton when residing at depth. Away from significant riverine influence, gradients in vertical turbulent mixing caused vertical advection towards areas of higher mixing. Vertical distributions of phytoplankton should be driven by an equilibrium between vertical advection and sinking velocity. However, turbulent mixing gradients changed on small timescales (< 30 seconds) and so an equilibrium could not be maintained. These results indicate that in areas where turbulent mixing is maintained for long time periods an equilibrium could form, such as the deep chlorophyll maxima.

Keywords: Phytoplankton, Turbulence, Vertical Distributions, Pigments.

Introduction

Sea levels are predicted to rise by 0.7 m by 2100, in 'worst' case models, due to climate change (IPCC, 2014). Estuaries, which tend to act as CO2 sources (Frankignoulle, et al., 1998; Chen & Borges, 2009) represent extensive habitats that are particularly vulnerable to rising sea levels and detailed understanding of physical and biological interactions is needed to predict responses to change.

Phytoplankton in estuaries drive the biological CO_2 sequestration pump through photosynthesis. Vertical and spatial distributions of phytoplankton in estuaries are driven not only by bottom up (nutrients, light) and top-down (grazing) controls but also by interactions of tidal currents, land drainage and topography.

In coastal (case II) waters, such as the Tamar Estuary, substances including suspended particulate matter (SPM), gelbstoff and phytoplankton compete for photosynthetically active radiation (PAR) in an optically complex environment (Morel & Prieur, 1977; Prieur & Sathyendranath, 1981; Gordon & Morel, 1983). In the Tamar estuary, both SPM and gelbstoff are in abundance (Sieburth & Jensen, 1968; Monahan & Pybus, 1978) and their differing absorption (Bricaud, et al., 1981) and scattering (Bowers, et al., 2009) properties change the spectrum of available light dynamically (Bowers, et al., 1997). The euphotic zone depth, usually defined as the 1% light level, is determined by the varying concentrations of different substances. This lowers the water volume that can support phytoplankton growth in the water column, as well as in the benthos.

The ability of phytoplankton to survive in the estuarine system spatially from mouth to head is dependent on tolerance to a wide range of salinities, and other environmental factors (Ahel, et al., 1996). This leads to a general spatial distribution of decreased concentrations in brackish waters (Lionard, et al., 2008; Gang, et al., 2014), where species composition starts to change due to environmental stress (Lancelot & Muylaert, 2011; Chai, et al., 2016). This change generally occurs in multiple steps between low salinity species in the upper estuary to marine species in the lower estuary, with low species richness in the brackish waters (Lionard, et al., 2008; Roubiex, et al., 2008). Phytoplankton are subjected to vertical mixing and stratification in the estuary, with well-mixed, low stratification conditions supporting lower, evenly distributed populations, and the converse where stratification is high (Cloern, 1991). Mixing can be driven through small scale turbulent motions (Osborn, 1980), which can determine the cell distribution in the water column (Macias, et al., 2013; Cross, et al., 2014). In estuaries, these motions are forced by the input of kinetic energy through tides and modulated by bathymetry. Phytoplankton are moved within and out of the euphotic zone through these small scale motions (Machado, et al., 2014).

In low light, phytoplankton may photo-acclimate both by increasing pigment concentrations without altering pigment ratios between chlorophyll-a (chl-a) and the accessory chlorophyll pigments (Geider, 1987) and acclimation by alteration of pigment ratios between chl-a and accessory pigments is also common (Roy, et al., 2011). Ratios between chl-a and chlorophyll-b (chl-b) has been found to decrease due to irradiance decreases, with an increase in chl-b (Falkowski & Owens, 1980).

In this study, the relationships between microstructure turbulence and phytoplankton distributions and pigmentation were investigated along the Tamar Estuary, UK. Four surveys were undertaken to collect vertical profiles of temperature, salinity, irradiance, shear microstructure and fluorescence to assess how the rate of turbulent dissipation of kinetic energy, ε, affects the concentration of phytoplankton in the water column.

Methods

The Tamar Estuary and River (Figure 1) is 31 km long from Plymouth Sound to Weir Head, with semi-diurnal tides. Mean tidal ranges throughout the survey period were 3.4 m, with maximum and minimum ranges of 5.6 m and 1.0 m (Figure 2) (Uncles & Stephens, 1990).

The estuary has 3 main sources of freshwater including the River Tamar above Weir Head and the rivers Tavy and Lynher. The River Tamar supplies the majority of this freshwater with the Tavy and Lynher providing about 30 and 20% respectively of the Tamar's input (Uncles & Stephens, 1990).

Meteorological data was accessed from Plymouth Marine Laboratory's (PML) meteorological station (Figure 1). Data was collected daily for the duration of the survey (Figure 2), which included wind speed and rainfall.

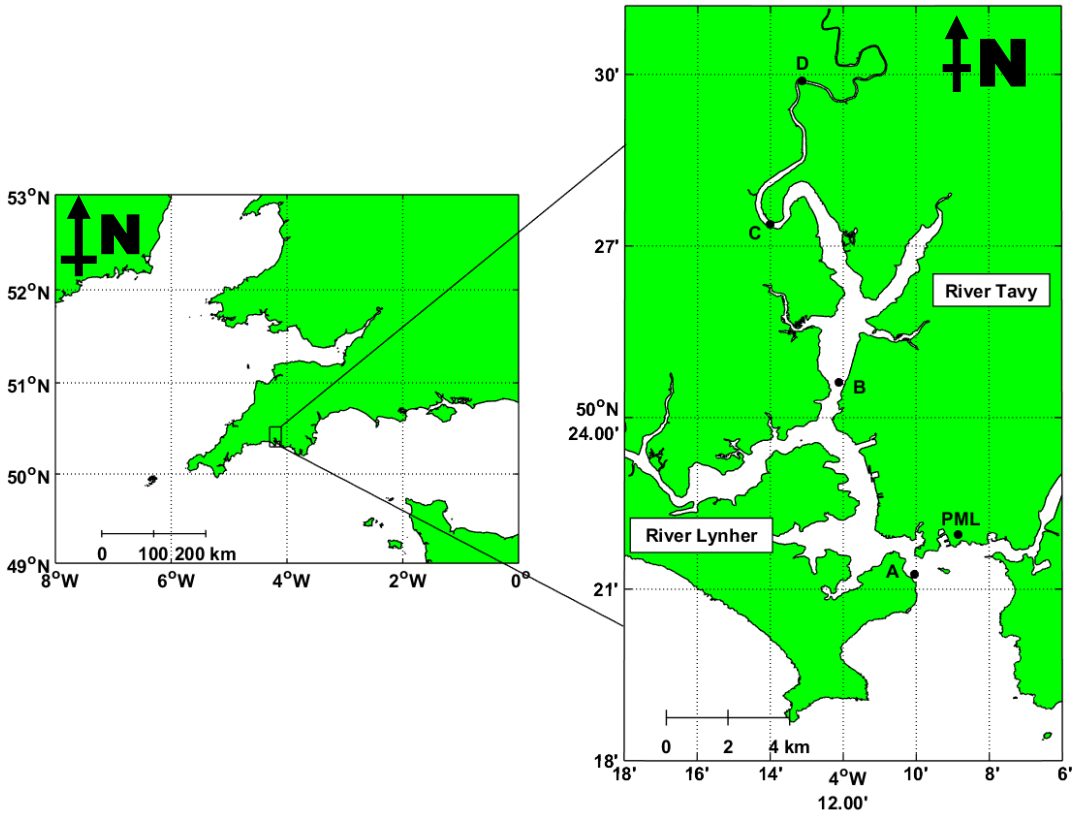

Figure 1: (left) Map of the UK, with insert indicating region of sampling location. (right) Map of the Tamar Estuary, displaying sampling locations (marked labels A-D), and also indicates PML weather station. (not displaying full extent to Weir Head)

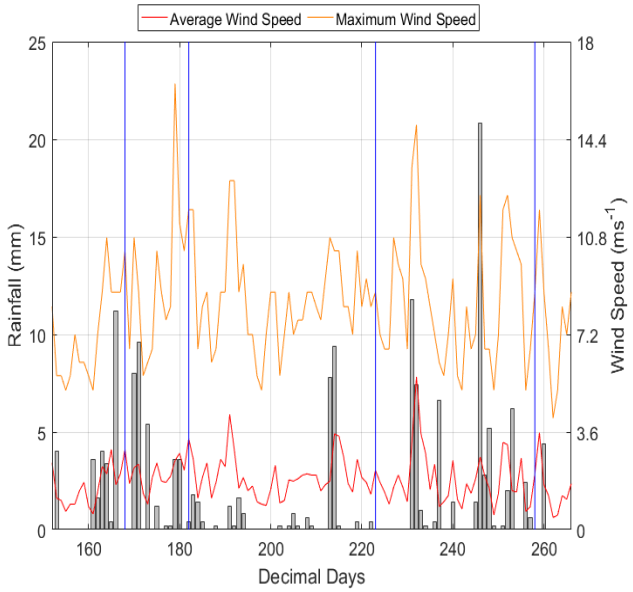

Figure 2: Meteorological data for the survey period collected at PML's meteorological station, indicating rainfall (inferring freshwater inputs) and wind speed before and during each survey. Vertical blue lines represent individual surveys.

Hydrodynamic Data

Surveys were conducted on a near monthly basis between June and September 2016, on two tidal states of neap ebb (NE; August - 224) and spring flood (SF; September - 259) (Table 1) to capture differing tidal energy inputs. An additional survey on the spring flood tide (SF2; July - 183) was also conducted. Station locations were chosen to ensure a minimum water depth of 5 m was obtained to allow for instrument deployment. Instrumentation and sensors are described in Appendix A.

Biospherical Instruments), sampling at 1 Hz, collected irradiance profiles simultaneously with CTD profiles. Surface irradiance was collected by a deck unit, such that changes in surface irradiance could be accounted for in the depth profiles.

The density profile can be represented by the square of the buoyancy frequency, N^2, calculated as;

$$N^2 = -\frac{g}{\rho_o}\frac{\Delta\rho}{\Delta z} \quad (1)$$

where g is the acceleration due to gravity, ρ_o is a reference density and $\Delta\rho/\Delta z$ the change in observed density with depth, z. The reference density for each profile was taken as the surface value.

The diffuse attenuation coefficient, K_d, was calculated for each of the PRR wavebands, centred on 412, 443, 488, 510, 560 and 665 nm. An additional PAR waveband was also used. K_d was determined from the linear regression of $\ln(E(z))$ against z, where E(z) is the irradiance at depth.

Table 1: Location and tidal information of stations surveyed on each tidal state. This includes the time around maximum neaps tides, the tidal state on the day each station was survey and the tidal range.

Survey Dates (Decimal Day)	**Station**	**Springs Flood** Neaps +5 days HW = 17.66 Tidal Range = 4.2 m	**Neaps Ebb** Neaps -2 days HW = 11.81 Tidal Range = 2.1 m
Spring Flood 15th September Day 259 Neap Ebb 11th August Day 224 Spring Flood 2 1st July Day 183	**A** (50° 21' 16.06'' N, 4° 10' 2.71'' W)	**HW -5.72h**	**HW +3.74h**
	B (50° 24' 36.81'' N, 4° 12' 7.76'' W)	**HW -0.03h**	**HW +2.36h**
	C (50° 27' 23.06'' N, 4° 14' 0.39'' W)	**HW -0.88h**	**HW +1.43h**
	D (50° 29' 53.71'' N, 4° 13' 7.62'' W)	**HW -1.65h**	**HW +0.05h**

The euphotic zone was defined as the water column above the 1% light level. This was calculated for the PAR waveband using the Beer Lambert Law (Kirk, 1994);

$$z_{1\%} = -\frac{Ln(0.01)}{K_d(PAR)} \quad (2)$$

The Microstructure Sensing System (MSS; ISW Wassermesstechnik*),* sampling at 1024 Hz*,* was deployed for three casts in short succession immediately after the CTD cast. The profiler was allowed to fall freely to within 1 m of the seabed. Profiler buoyancy was controlled by buoyancy and weight rings, with a single adjustment required at salinities below 5 giving fall speeds of 0.5 – 0.7 ms^{-1}. Estimates of ε were derived using the density overturn method (Thorpe, 1977; Appendix B) and using the turbulent shear data (Osborn, 1980; Appendix C). Parameters were averaged across the three casts.

The vertical turbulent motions were then characterised by the diapycnal diffusivity, K_ν, computed as;

$$K_\nu = \Gamma_o \frac{\varepsilon}{N^2} \quad (3)$$

(Osborn, 1980). The mixing efficiency, Γ_o, was taken as 0.2 but can range between 0.05 to 0.7 in ocean systems (Yamazaki & Osborn, 1993; Gargett & Moum, 1995).

Chlorophyll Analysis

Water samples were collected from the surface and 1 m from the seabed with a van Dorn water sampler. These were frozen for a maximum of 3 weeks before analysis. Analysis followed Strickland and Parsons (1972) with modifications: Instead of

centrifuging, silicon-zirconia beads were added to the vial and the sample, with 0.24 ml of 90% acetone, agitated in a beadbeater (Mini Beadbeater TM, Biospec Products) until the filter had disintegrated. The pulp was then filtered through a 0.2 µm filter into the 1 cm cuvette.

Spectra were recorded between 350 – 750 nm, at 2 nm bandwidth, to calculate chl-a and chl-b concentrations using trichromatic equations derived by Jeffery & Humphrey (1975);

$$C_a = 11.85A_{664} - 1.54A_{647} - 0.08A_{630} \quad (4)$$
$$C_b = 21.03A_{647} - 5.43A_{664} - 2.66A_{630}$$

where A_λ is the absorbance value at wavelength λ nm. Some spectra included a detritus signal that was removed by calculating an exponential curve between 350 to 750 nm using equation 5;

$$A_\lambda = A_{350} * e^{-\sigma(\lambda-350)} \longrightarrow \sigma = -\frac{\ln(A_{750} / A_{350})}{750-350} \quad (5)$$

where A_λ and A_{350} are absorbance values. σ is the spectral slope of this curve, and was determined as in equation 5.

Chl-a measurements from discrete water samples were used to produce calibration curves for both fluorometers (see Appendix D).

Results and Discussion

Irradiance and Light Availability

Surface irradiance for the spring flood (SF) were ~10% of the neap-ebb (NE) values due to increased cloud cover (Figure 3B).

For both tidal periods, K_d increased from station A to D with the strongest attenuation, 6.5 m^{-1}, at 412 nm, observed at station D (Figure 3A). Kd was 0.3 m^{-1} higher on the SF compared to the NE conditions at stations A and B. A greater difference of 1.2 m^{-1} was observed at station C. Values at station D could not be compared as light had attenuated below the PRR detection limit within the first 0.5 m on the SF.

The attenuation spectrum was flattest at station A on both tides. Between stations A and D the attenuation increased near linearly for the red (560 and 665 nm) light, indicating an increase in scattering from suspended particulate matter (Bowers, et al., 2009). A significant correlation was found between K_d(665 nm) and suspended particulate matter (R^2 = 0.8735, $p < 0.01$, n = 10) consistent with an increase in particulate scattering. Attenuation in blue wavebands (412 and 443 nm) increased markedly from station A to D. K_d(412 nm) > K_d(443 nm) at stations A, B and D suggested an increase in gelbstoff concentrations in the fresher water (Kirk, 1994), in contrast to station C where relatively higher K_d(443) would indicate a chl-a signature.

The increase in light attenuation moving upstream from station A causes a shoaling of the euphotic depth, from >10 m to 3 m, and $z_{1\%}$ did not exceed the bottom depth at any station (Figure 3B).

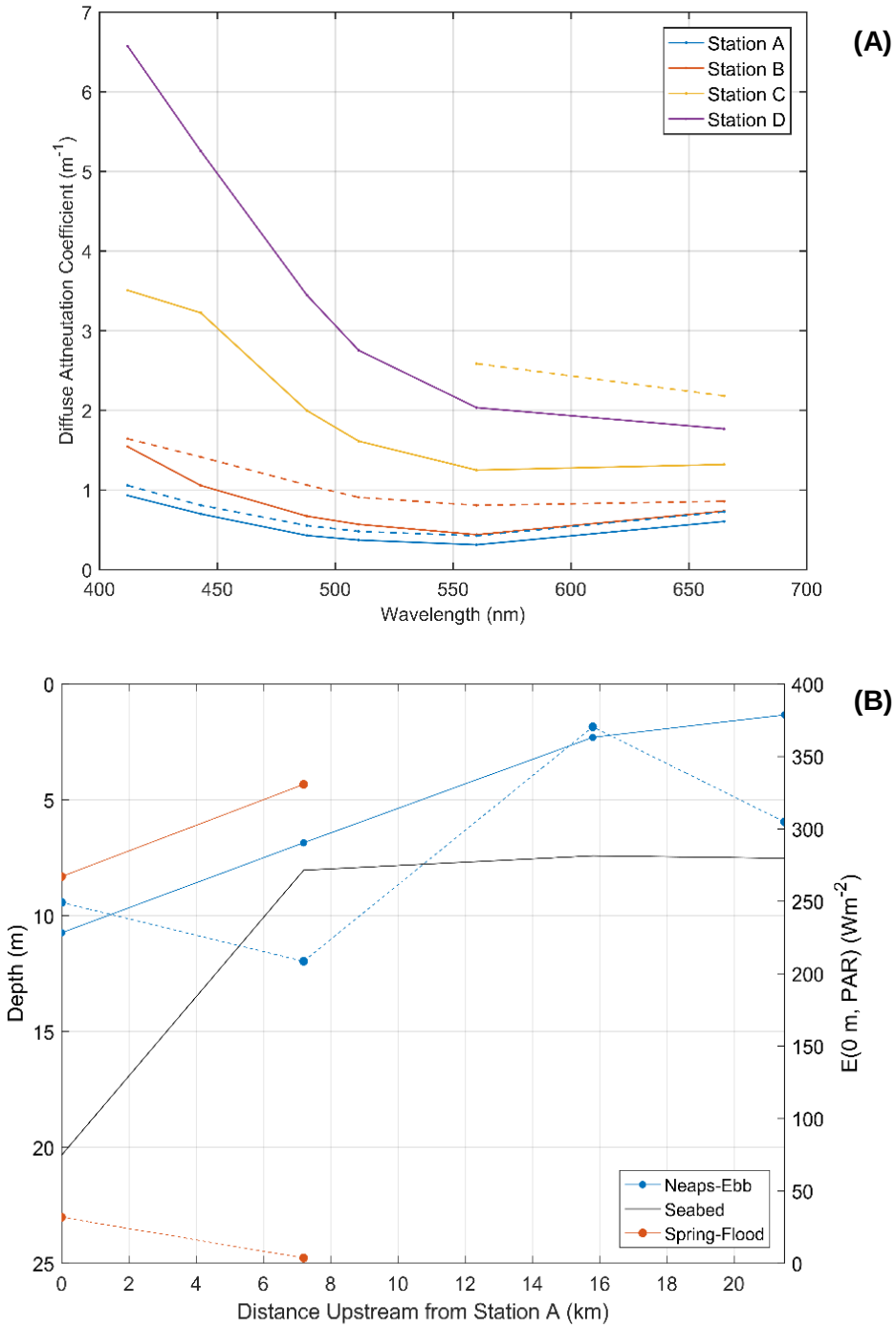

Figure 3: (A) Diffuse Attenuation Coefficient (K_d) displayed for each of the six PRR wavebands, for each station surveyed. Solid line is the survey on the neaps-ebb (NE), and the dashed line is the springs-flood (SF). Lines that aren't present or are partially present indicate where irradiance was attenuated to below the PRR's sensitivity in the first 0.5 m. **(B)** Euphotic zone depth calculated as the 1% light level for PAR, for both the Spring Flood (Orange) and the Neaps Ebb (Blue). Points not present indicate areas where light was attenuated such that K_d could not be calculated. Black line indicates depth of the seabed. Dashed lines indicate the surface PAR irradiance for each station, and corresponding tide.

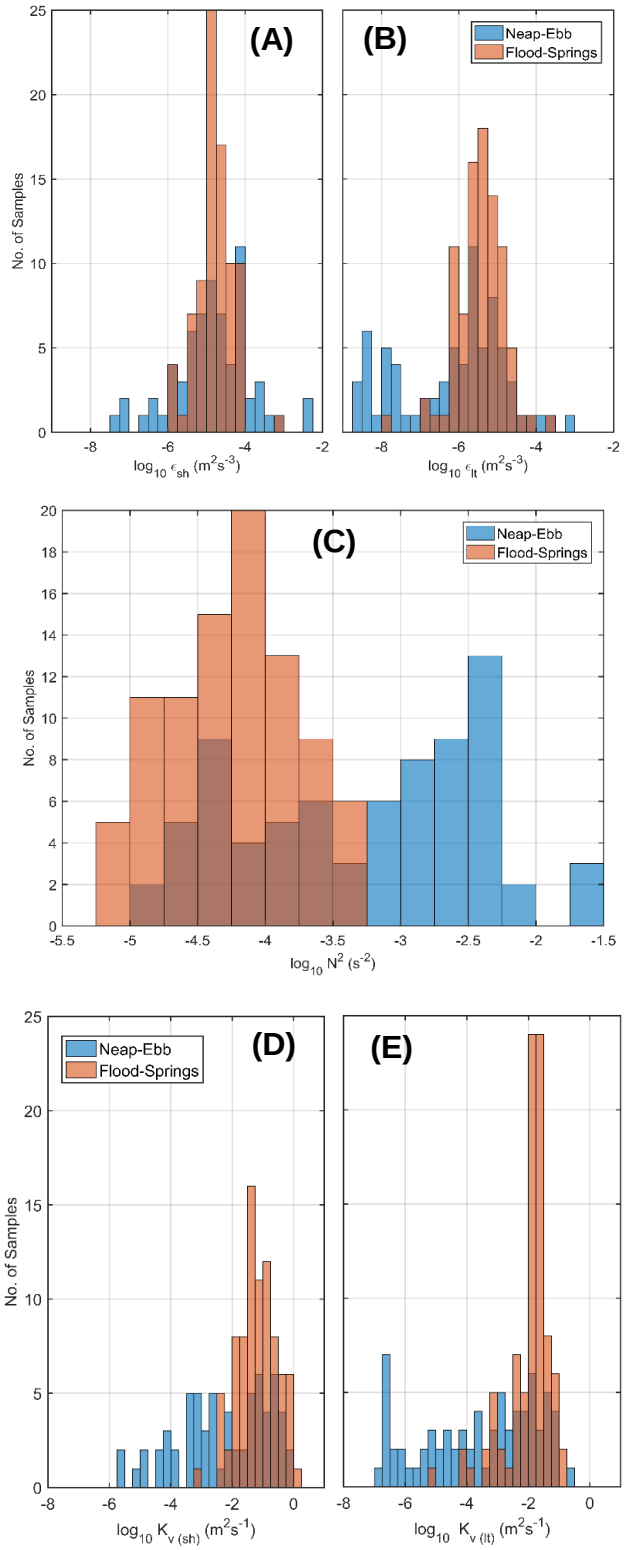

Figure 4: (A) Number of samples per $\log_{10}$ 0.25 bin of ε for the two tidal states, flood-springs (orange) and ebb-neaps (blue), estimated from MSS shear data. **(B)** Same as (A) but ε estimated through Thorpe scales. **(C)** Number of samples per $\log_{10}$ 0.25 bin of N^2 for the two tidal states calculated from CTD density profiles. **(D)** Number of samples per $\log_{10}$ 0.25 bin of K_v for the two tidal states calculated using MSS shear estimated ε. **(E)** Same as (D) but calculated using Thorpe scale estimated ε.

Temporal distributions of ε, N^2 and Kv

As the CTD sampling frequency (4 Hz) was too low to resolve the microstructure density inversions that the density overturn method requires, estimates of ε were made with the MSS shear data (ε_{sh}) and MSS density profiles (ε_{lt}). ε, N^2 and K_v values for NE and SF are shown in Figure 4. ε_{sh} spanned similar orders of magnitude (Figure 4A) for the two tidal states though with greater variations in ε_{sh} during NE, with values ranging from $10^{-8} < \varepsilon_{sh} < 10^{-3}$ m^2s^{-3} compared to $10^{-6} < \varepsilon_{sh} < 10\text{-}4$ m^2s^{-3} for the SF. A similar trend was found for ε_{lt} (Figure 4B) however a larger number of values below 10^{-7} m^2s^{-3} was found in NE in a possible bimodal distribution with maxima at O($10^{-8.5}$ m^2s^{-3}) and O($10^{-5.5}$ m^2s^{-3}). ε_{sh} was on average O(10^{-5} m^2s^{-3}) throughout both tidal states; an order of magnitude higher than the values determined through Thorpe scales.

The wider range of ε on the NE is consistent with previous studies (Peters & Bokhorst, 2000), where the enhanced dissipation rates due to tidal forcing are supressed to below the pycnocline, leading to enhanced ε at the seabed, and near constant ε in the remaining water column. The smaller range in ε on the SF is consistent with Peters and Bokhorst (2000) although their values were higher at O($10^{-4.5}$ m^2s^{-3}).

N^2 ranged from $10^{-5} < N^2 < 10^{-1.5}$ s^{-2} during the NE (Figure 4C), indicating high spatial variability in stratification. A lower range of $10^{-5.5} < N^2 < 10^{-3.25}$ s^{-2} was found for SF.

ε on both tidal states was on average O(10^{-5} m^2s^{-3}) indicating that K_v was predominately controlled by N^2. K_v was calculated for both estimates of ε, leading to parameters $K_{v\,(sh)}$ and $K_{v\,(lt)}$ for the respective estimation methods.

SF showed higher values of K_v (Figure 4D, 4E) ranging from O($10^{-3} < K_{v\,(sh)} < 10^{0}$ m^2s^{-1}). These enhanced values indicated more rapid mixing due to turbulent motions that are not suppressed by stratification. A larger range of O($10^{-7} < K_{v\,(sh)} < 10^{-1}$ m^2s^{-1}) was found for NE. $K_{v\,(lt)}$ spanned the same range with an order of magnitude decrease.

Spatial distributions of ε, N^2 and K_v

ε remained constant throughout the water column at all four stations, except at the surface and the seabed. Surface ε were generally an order of magnitude higher, with the seabed either an order of magnitude higher or lower, reinforcing stratification-driven K_v.

N^2 indicated increased stratification moving from Station A to D, on both tidal states (Table 2). SF had N^2 O(10^{-4} s^{-2}) throughout all stations except station D where an increase to O(10^{-3} s^{-2}) was observed.

Station A on the NE showed a similar order of magnitude to the SF. Stations B, C and D compared to the SF showed a minimum increase of an order of magnitude on the NE.

Changes in K_v were examined in terms of $K_{v\,(sh)}$ where $K_{v\,(lt)}$ was an order of magnitude lower. K_v showed a reversed trend spatially to N^2 where station A had highest K_v at $O(10^{-1}\ m^2s^{-1})$ on the NE. K_v decreased from station A to D with a minimum of $O(10^{-3}\ m^2s^{-1})$ at station D. On the SF stations B and C displayed higher K_v at $O(10^{-1}\ m^2s^{-1})$, with an order of magnitude decrease at both stations A and D.

Table 2: Spatial and temporal distributions in both K_v and N^2 for each station on both the Neaps Ebb and Spring Flood. Results here reinforce that differences in K_v between stations (and surveys) are largely controlled by changes in N^2.

Station	Neap Ebb		Spring Flood	
	$\log_{10} K_{v\,(sh)}$ (m^2s^{-1})	**$\log_{10} N^2$ (s^{-2})**	**$\log_{10} K_{v\,(sh)}$ (m^2s^{-1})**	**$\log_{10} N^2$ (s^{-2})**
A	-0.88 ± 1.09	-3.88 ± 0.65	-1.02 ± 0.61	-4.16 ± 0.36
B	-1.38 ± 1.31	-2.46 ± 0.15	-0.56 ± 0.45	-4.61 ± 0.47
C	-1.84 ± 0.72	-2.62 ± 0.77	-0.82 ± 0.63	-4.13 ± 0.32
D	-2.50 ± 0.42	-2.94 ± 0.69	-1.49 ± 0.43	-3.63 ± 0.20

This demonstrates the reduced vertical mixing due to turbulent motions, and increased water column stability, on the NE as seen in previous studies (Cloern, 1991; Peters, 1997).

Phytoplankton and K_v

The amount of vertical mixing due to turbulent motions determines the vertical structure and concentration of chl-a in the water column (Figure 5A; $R^2 = 0.8582$, $p < 0.01$, $n = 12$). As the average water column K_v decreases, chl-a concentrations in the surface 1 m increased. The ratio between the surface 1 m total chl-a and the total water column chl-a decreased exponentially with increasing K_v. This was observed as a homogenisation of the water column chl-a concentrations. Low K_v conditions reduce phytoplankton sinking velocities (Ruiz, et al., 2004), and mixing is slow, such that phytoplankton remain in the euphotic zone. Cells are not redistributed through the water column and vertical chl-a distributions maximise productivity in the water column (Tilzer & Goldman, 1978). In turbid waters, chl-a profiles are expected to follow the exponential decrease in irradiance with increasing depth to a background chl-a concentration. Increased K_v causes chl-a in the surface waters to be mixed due to increased sinking speeds (Ruiz, et al., 2004), so that chl-a concentrations become near homogenous with depth. This is consistent with Cloern (1991), who used a homogenous water column K_v model that incorporated changing K_v due to spring-neap tidal cycles. Increased surface chl-a concentrations shortly after neap tides were found due to low K_v. During spring tides, increased K_v dispersed phytoplankton cells. Increased ε and decreased N^2 (used to infer increased K_v), due to increased wind forcing can also disperse phytoplankton on shorter timescale (hours) (Cross, et al., 2014).

The chl-a / chl-b ratio at the surface was also related to K_v (Figure 5B; $R^2 = 0.7146$, $p = 0.0135$, $n = 12$). Increased K_v was found to be associated with a

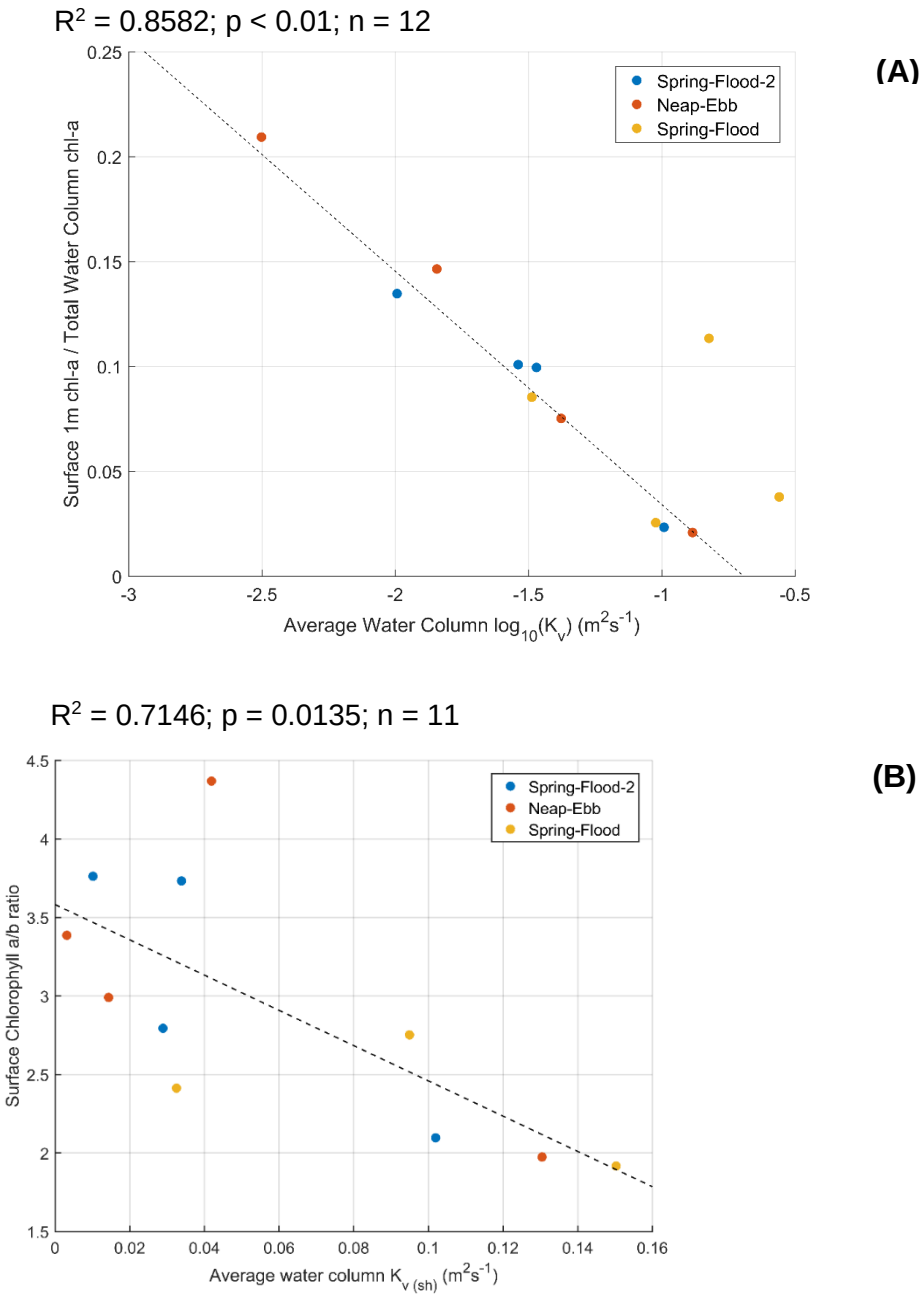

Figure 5: (A) Average water column $\log_{10}(K_v)$ across the three surveys scattered against the surface 1 m chl-a to total water column chl-a ratio. This indicates as turbulent mixing increases the water column chl-a becomes more homogenous. If K_v is low, chl-a profiles show higher concentrations in the surface. **(B)** Average water column K_v against the surface chl-a / chl-b ratio. Indicating an increase in the ratio as mixing is decreased, where phytoplankton stay at the surface. As K_v increases phytoplankton from the surface are mixed through the euphotic zone and so the ratio decreases as photoacclimation occurs.

decrease in the ratio, indicating photoacclimation of phytoplankton to the irradiance conditions. Low K_v causes phytoplankton to be slowly mixed, remaining in similar irradiance conditions for long time periods (Cullen & Lewis, 1988). Irradiance at the surface has undergone limited spectral change (in <10 cm of water), such that chl-a remains an effective pigment for light harvesting. Increased mixing, as K_v increases, moves phytoplankton throughout the euphotic zone, and below. Irradiance at depth has undergone varied attenuation across the PAR spectrum (Figure 3A) such that chl-a absorption below 500 nm has limited efficiency. Photoacclimation through pigmentation changes as phytoplankton reside at depth decreases the chl-a/chl-b ratio before cells are reintroduced to the surface (Falkowski & Owens, 1980; Cullen & Lewis, 1988). It must be noted that this pigmentation change could also indicate a species composition change when moving from marine to freshwaters (Lancelot & Muylaert, 2011), as was observed by Chai, et al (2016) in the Pearl River Estuary. However, salinity has limited effect on the chl-a/chl-b ratio (Figure 6; $R^2 = 0.2471$, $p = 0.4638$, $n = 11$), indicating a species composition change isn't significantly affecting the ratio. Similar observations of the chl-a / chl-b ratio from phytoplankton near the seabed showed no statistically significant correlation ($R^2 = 0.3564$, $p = 0.2820$, $n = 11$) between the chl-a / chl-b ratio and K_v.

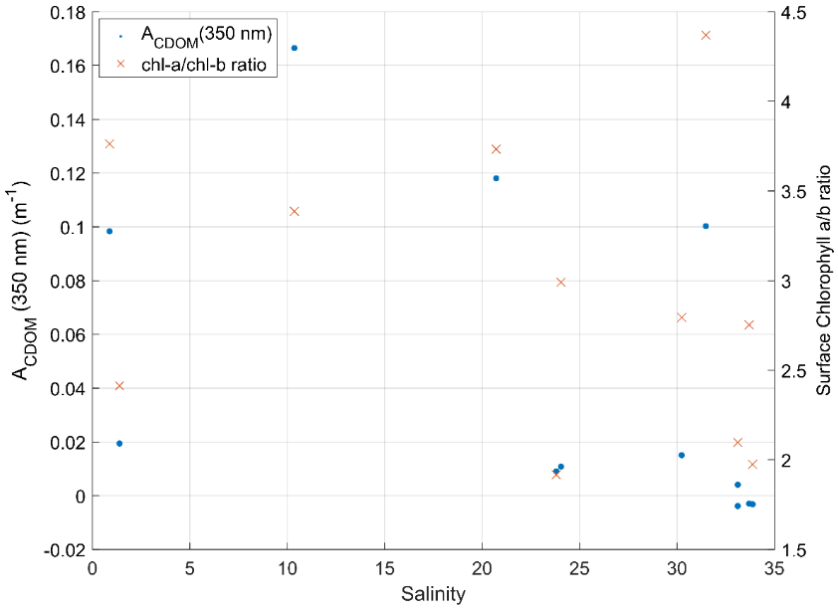

Figure 6: chl-a/chl-b ratio (crosses) against salinity to evaluate if a species composition change influenced the distribution in phytoplankton pigments. No statistical correlation was found between the two ($R^2 = 0.2471$, $p = 0.4638$, $n = 11$), indicating a species composition change had limited effect on the chl-a/chl-b ratio. A_{CDOM}(350 nm) was also plotted to demonstrate the change in riverine influence across the salinity range ($R^2 = 0.500$, $p = 0.093$, $n = 12$). Indicating the near 0 absorbance in the higher salinities as found at station A, suggesting limited riverine optical properties.

Mixing below the euphotic zone would initially drives an increase in pigmentation per cell as a photo-adaptive response followed by a decrease in pigments, due to pigment decomposition, unless phytoplankton are reintroduced to the euphotic zone prior to cell death (Tilzer, et al., 1977). If mixed below the euphotic zone for 30 days, a decrease in chl-a concentrations in phytoplankton of around 50% was observed by Tilzer, et al. (1977).

Phytoplankton and gradients in K_v

To examine phytoplankton pigment concentration and gradients in K_v vertically, station A was used as it had the greatest water depth and negligible riverine optical properties. No correlation was found pigment concentrations and gradients in K_v when examining averaged MSS profiles (not shown).

K_v and chl-a concentrations changed on small time periods (<30 seconds) between the three averaged profiles (Figure 7A). Individual MSS profiles showed variations in K_v of as much as three orders of magnitude. Similarly, chl-a concentrations could vary by as much as 1 mgm^{-3}.

Applying the same process to individual profiles, gradients in K_v was associated with a change in chl-a concentrations (Figure 7B; $R^2 = 0.1384$, $p = 0.0112$, $n = 335$), where positive gradients were attributed to positive increases in chl-a. A reciprocal change was seen with negative gradients. This suggests that concentrations of chl-a are increased, due to convergence, at areas of higher K_v. This is counter intuitive if increased sinking velocities from higher K_v (Ruiz, et al., 2004) were the sole driver of the distribution.

Visser (1997) examined this process through modelling K_v and phytoplankton. Advection from lower to higher K_v areas due to differences in the kinetic energy of the eddies introduces a net motion towards higher K_v (Hunter, et al., 1993), thus driving distributions. Due to advection the peak in chl-a would occur where the net advection and phytoplankton sinking velocities (Ruiz, et al., 2004) are balanced, offsetting the peak in chl-a from the peak in K_v. In the deep ocean, the deep chlorophyll maxima (DCM) are consistently observed below the peak in K_v (and ε) (Macias, et al., 2013), reinforcing this theory. The weak correlation for this process (Figure 7B) is likely due to the timescale at which K_v was maintained. Figure 7A shows K_v changes on timescales of 30 seconds, if not smaller, indicating a low temporal memory for turbulence (Pelegri & Sangra, 1998). Thus the advection of phytoplankton is unable to reach an equilibrium state with the sinking velocity. The DCM must partially be maintained by a high temporal memory for turbulence, where changes can cause instabilities to form (Huisman, et al., 2006). This indicates a long temporal memory for turbulence must occur for distributions to reach equilibrium.

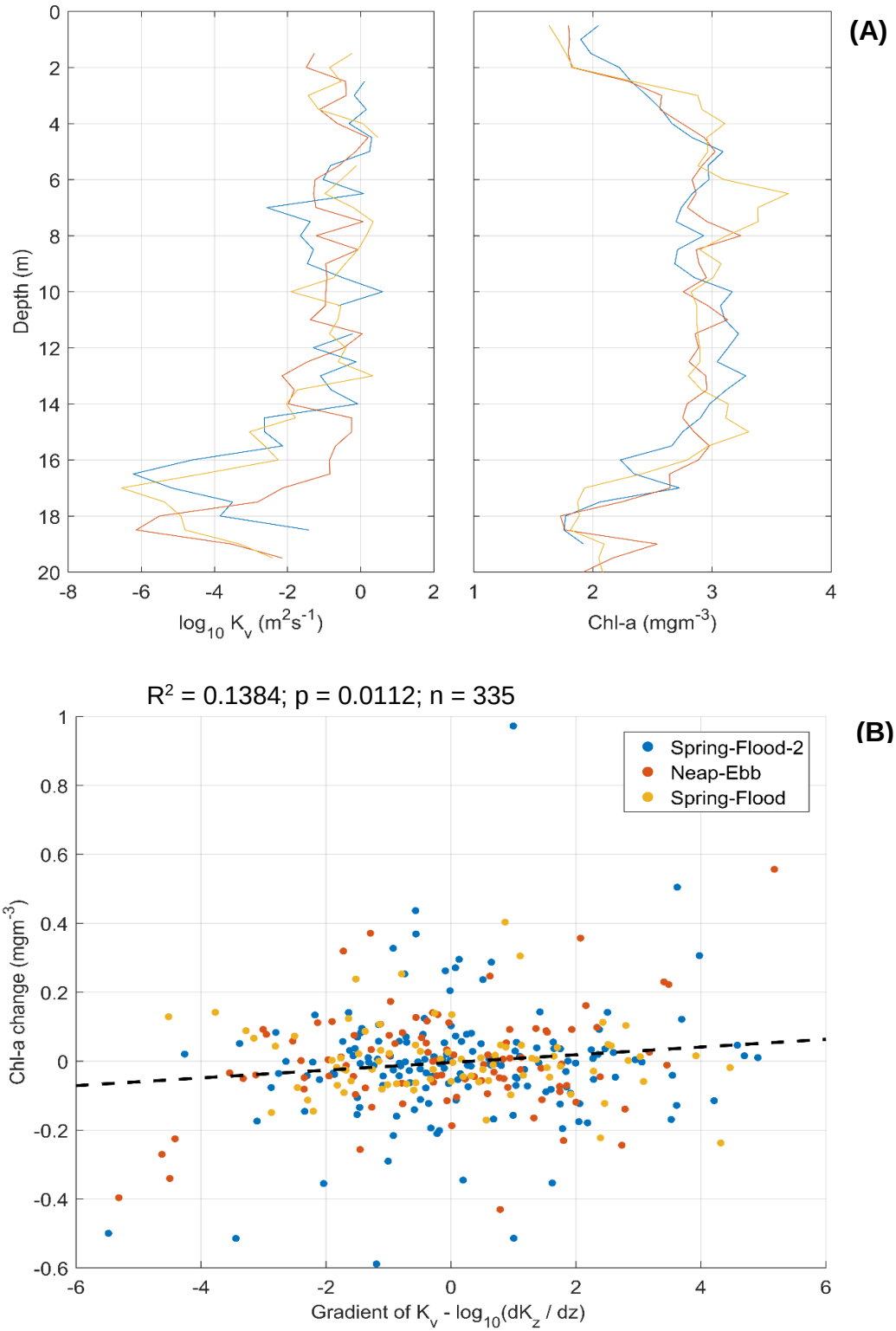

Figure 7: (A) Three repeat MSS casts for station A on the SF survey, to indicate the variability on <30 second time scales of both K_v (left panel) and chl-a profiles (right panel). Each profile is ~30 seconds apart in the order; Blue, Orange to Yellow. **(B)** The effect of gradients in K_v on chl-a in the water column. Positive gradients in K_v indicate an increase in K_v moving towards the surface where negative gradients indicate the opposite.

Conclusions

Turbulent mixing is shown, to be a parameter that controls phytoplankton vertical distributions. Low K_v allows chl-a concentrations to increase in the surface waters. High K_v causes surface chl-a to become homogenised throughout the water column. This reinforces results from previous studies (Cloern, 1991; Cross, et al., 2014).

Changes in the chl-a/chl-b ratio observed also reinforce this interpretation of mixing. Phytoplankton that are mixed slowly, and remain in the surface waters, (low K_v) have a higher chl-a/chl-b ratio due to limited spectral change in the irradiance they reside in. Higher mixing (high K_v) causes phytoplankton to be mixed throughout the euphotic zone. Varied attenuation over the PAR spectrum causes a spectral change in the irradiance that negatively impacts the efficiency of chl-a, such that photoacclimation decreases the ratio before phytoplankton are reintroduced to the surface.

Gradients in K_v determine the vertical distribution of phytoplankton. An equilibrium between sinking velocities and advection to higher K_v areas drives vertical distributions. However, K_v fluctuated on time periods <30 seconds which prevented an equilibrium from forming and a weak correlation was found between the gradient in K_v and chl-a concentrations.

Further research is required throughout areas of differing temporal variabilities of K_v, to determine whether an equilibrium between advection and sinking velocity can be maintained. Improving the resolution at which ε can be determined would allow for a finer scale determination of this equilibrium, although this requires improvements to instrumentation. Measurement of primary productivity as well as a wider range of accessory photosynthetic and photo-adaptive pigments would aid interpretation of the phytoplankton response to turbulence in coastal waters. Numerical models would benefit from further investigation to better model changes in estuaries due to sea level rise.

Acknowledgements

The meteorological data were provided by the NERC National Capability funded Western Channel Observatory. Many thanks also to Dr Jill Schwarz for support and guidance throughout, to Dr Phillip Hosegood for use of the MSS and to Jonathan Coe, Richard Skinner and Richard Kenyon for assisting in data collection.

References

Ahel, M., Barlow, R. G. & Mantoura, R. F. C., 1996. Effect of salinity gradients on the distribution of phytoplankton pigments in a stratified estuary. *Mar. Eco. Prog. Ser.,* Volume 143, pp. 289-295, doi: 10.3354/meps143289.

Bowers, D. G., Braithwaite, K. M., Nimmo-Smith, W. A. M. & Graham, G. W., 2009. Light scattering by particales suspended in the sea: The role of particle size and density. *Continental Shelf Research,* Volume 29, pp. 1748-1755, doi: 10.1016/j.csr.2009.06.004.

Bowers, D. G., Tett, P. & Walne, A. W., 1997. A note on seabed irradiance in shallow tidal seas. *Jou. Mar. Bio. Ass. UK,* 77(4), pp. 921 - 928, doi: 10.1017/S0025315400038534.

Bricaud, A., Morel, A. & Prieur, L., 1981. Absorption by dissolved organic matter of the sea (yellow substance) in the UV and visible domains. *Limnol. Oceanogr.,* Volume 26, pp. 43-53, doi: 10.4319/lo.1981.26.1.0043.

Campbell, J. W., 1995. The lognormal distribution as a model for bio-optical variability in the sea. *Jour. Geoph. Res.,* 100(C7), pp. 13237-13254, doi: 10.1029/95JC00458.

Chai, C. et al., 2016. Phytoplankton pigments and functional community structure in relation to environmental factors in the Pearl River Estuary. *Oceanologia,* 58(3), pp. 201-211, doi: 10.1016/j.oceano.2016.03.001.

Chen, C. T. A. & Borges, A. V., 2009. Reconciling opposing views on carbon cycling in the coastal ocean: Continental shelves as sinks and near-shore ecosystems as sources of atmospheric CO2. *Deep-Sea Res. II,* Volume 56, pp. 578-590, doi: 10.1016/j.dsr2.2009.01.001.

Cloern, J. E., 1991. Tidal stirring and phytoplankton bloom dynamics in an estuary. *J. of Mar. Res.,* Volume 49, pp. 203-221, doi: 10.1357/002224091784968611.

Cross, J., Nimmo-Smith, W. A. M., Hosegood, P. J. & Torres, R., 2014. The dispersal of phytoplankton populations by enchance turbulent mixing in a shallow coastal sea. *J. Mar. Sc.,* Volume 136, pp. 55-64, doi: 10.1016/j.jmarsys.2014.03.009.

Cullen, J. J. & Lewis, M. R., 1988. The kinetics of algal photoadaptation in the context of vertical mixing. *Jou. Plank. Res.,* 10(5), pp. 1039-1063, doi: 10.1093/plankt/10.5.1039.

Dillon, T. M., 1982. Vertical Overturns: A comparison of Thorpe and Ozmidov length scales. *J. of Geophysical Res.,* Volume 87, pp. 9601-9613, doi: 10.1029/JC087iC12p09601.

Falkowski, P. G. & Owens, T. G., 1980. Light-shade adaptations: two strategies in marine phytoplankton. *Plant Physiol.,* Volume 66, pp. 592-595, doi: 10.1104/pp.66.4.592.

Frankignoulle, M. et al., 1998. Carbon Dioxide Emission from European Estuaries. *Science,* Volume 282, pp. 434-436, doi: 10.1126/science.282.5388.434.

Gang, L. et al., 2014. Environmental gradients regulate the spatial variations of phytoplankton biomass and community structure in surface water of the Pearl River estuary. *Acta Ecologica Sinica,* Volume 34, pp. 129-133, doi: 10.1016/j.chnaes.2014.01.002.

Gargett, A. E. & Moum, J. N., 1995. Mixing effciencies in turbulent tidal fronts: Results from direct and indirect measurments of density flux. *J. Phys. Oceanogr.,* Volume 25, pp. 2583-2608, doi: 10.1017/jfm.2017.36.

Gargett, A. E., Osborn, T. R. & Nasmyth, P. R., 1984. Local isotropy and the decay of turbulence in a stratified fluid. *Jou. Fluid Mech.,* Volume 144, pp. 231-280, doi: 10.1017/S0022112084001592.

Geider, R. J., 1987. Light and Temperature dependence of the carbon to chlorophyll-a ratio in microalgae and cyanobacteria: implications for physiology and growth of phytoplankton. *New Phytol.,* Volume 106, pp. 1-34, doi: 10.1111/j.1469-8137.1987.tb04788.x.

Gordon, H. R. & Morel, A. Y., 1983. Remote assessment of ocean colour for interpretation of satellite visible imagery. A review.. *New York: Springer,* Volume 81, pp. 198, doi: 10.1029/LN004.

Huisman, J., Pham Thi, N. N. N., Karl, D. M. & Sommeijer, B., 2006. Reduced mixing generates oscillations and chaos in the oceanic deep chlorophyll maximum. *Nature,* Volume 439, pp. 322 - 325, doi: 10.1038/nature04245.

Hunter, J. R., Craig, P. D. & Phillips, H. E., 1993. On the use of random walk models with spatially variable diffusivity. *J. Comput. Phys.,* Volume 106, pp. 366-376, doi: 10.1016/S0021-9991(83)71114-9.

IPCC, 2014. *Climate Change 2014: Synthesis Report. Contribution of Working Groups I, II and III to the Fifth Assessment Report of the.* Core Writing Team, R.K. Pachauri and L.A. Meyer (eds.) ed. Geneva, Switzerland: IPCC.

Jeffery, S. & Humphrey, G., 1975. New Spectrophotometric Equations for Determining Chlorophylls a, b, c + c in Higher Plants, Algae and Natural Phytoplankton. *Biochem. Physiol. Pflanzen. Bd,* Volume 167, pp. 191-194, doi: 10.1016/S0015-3796(17)30778-3.

Kirk, J., 1994. *Light and Photosynthesis in Aquatic Ecosystems.* 2nd ed. Cambridge: Cambridge University Press.

Lancelot, C. & Muylaert, K., 2011. Trends in estuarine phytoplankton ecology. In: E. Wolanski, et al. eds. *Treatise on Estuarine and Coastal Science: 7. Functioning ecosystems at the land-ocean interface.* Amsterdam: Elsevier, pp. 5-15, doi: 10.1016/B978-0-12-374711-2.00703-8.

Lionard, M. et al., 2008. Inter-annual variability in phytoplankton summer blooms in the freshwater tidal reaches of the Schelde estuary (Belgium). *Estuarine, Coastal and Shelf Science,* Volume 79, pp. 694-700, doi: 10.1016/j.ecss.2008.06.013.

Machado, D. A., Marti, C. L. & Imberger, J., 2014. Influence of microscale turbulence on the phytoplankon of a temperate coastal embayment, Western Australia. *Estuarine Coastal and Shelf Science,* Volume 145, pp. 80-95, doi: 10.1016/j.ecss.2014.04.018.

Macias, D. et al., 2013. Turbulence as a driver for vertical plankton distribution in the subsurface upper ocean. *Scientia Marina,* 77(4), pp. 541-549, doi: 10.3989/scimar.03854.03A.

Monahan, E. C. & Pybus, M. J., 1978. Colour, ultraviolet absorbance and salinity of the surface waters off the west coast of Ireland. *Nature,* Volume 274, pp. 782-784, doi: 10.1038/274782a0.

Morel, A. & Prieur, L., 1977. Analysis of variations in ocean colour. *Limnol. Oceanogr.,* Volume 22, pp. 709-722, doi: 10.4319/lo.1977.22.4.0709.

Osborn, T. R., 1980. Estimates of the local rate of vertical diffusion from dissipation measurements. *J. of Phys. Oceano.,* Volume 10, pp. 83-89, doi: 10.1175/1520-0485(1980)010<0083:EOTLRO>2.0.CO;2.

Pelegri, J. L. & Sangra, P., 1998. A mechanism for layer formation in stratified geophysical flows. *J. Geophys. Res.,* Volume 103, pp. 30679-30693, doi: 10.1029/98JC01627.

Peters, H., 1997. Observations of Stratified Turbulent Mixing in an Estuary: Neap-to-spring Variations During High River Flow. *Estuarine, Coastal and Shelf Science,* Volume 45, pp. 69-88, doi: 10.1006/ecss.1996.0180.

Peters, H. & Bokhorst, R., 2000. Microstructure Observations of Turbulent Mixing in a Partially Mixed Estuary. Part I: Dissipation Rates. *J. Phys. Oceanog.,* Volume 30, pp. 1232-1244, doi: 10.1175/1520-0485(2000)030<1232:MOOTMI>2.0.CO;2.

Prieur, L. & Sathyendranath, S., 1981. An optical classification of coastal and oceanic waters based on the specific spectral absorption curves of phytoplankton pigments, dissolved organic matter and other particulate matter. *Limnol. Oceanogr.,* Volume 26, pp. 671-689, doi: 10.4319/lo.1981.26.4.0671.

Roubiex, V., RousseaumV. & Lancelot, C., 2008. Diatom succession and silicon removal from freshwater in estuarine mixing zones: from experiment to model. *Estuarine, Coastal and Shelf Science,* Volume 78, pp. 14-26.

Roy, S., Llewellyn, C. A., Egeland, E. S. & Johnsen, G., 2011. *Phytoplankton Pigments: Characterixation, Chemotaxononmy and Applications in Oceanography.* Cambridge: Cambridge University Press, doi: 10.1111/jpy.12035.

Ruiz, J., Macias, D. & Peters, F., 2004. Turbulence increases the average settling velocity of phytoplankton cells. *Proceedings of the National Academy of Sciences,* Volume USA 101, pp. 17720-17724, doi: 10.1073/pnas.0401539101.

Sieburth, J. M. & Jensen, A., 1968. Studies on algal substances in the sea. I. Gelbstoff (humic material) in terrestrial and marine waters. *J. Exp. Mar. Biol. Ecol.,* Volume 2, pp. 174-189, doi: 10.1016/0022-0981(68)90008-7.

Strickland, J. D. H. & Parsons, T. R., 1972. *A practical handbook of seawater analysis.* 2nd ed. Ottawa: Fish. Res. Board. Can. Bull..

Thorpe, S. A., 1977. Turbulence and Mixing in a Scottish Loch. *Philosophical Transactions of the Royal Society of London. Series A, Mathematical and Physical Sciences,* Volume 286, pp. 125-181, doi: 10.1098/rsta.1977.0112.

Tilzer, M. M. & Goldman, C. R., 1978. Importance of mixing, themal stratification and light adaptation for phytoplankton productivity in Lake Tahoe (California-Nevada). *Ecology,* Volume 59, pp. 810-821, doi: 10.2307/1938785.

Tilzer, M. M., Paerl, H. W. & Goldman, C. R., 1977. Sustained viability of aphotic phytoplankton in Lake Tahoe (California-Nevada). *Limnology and Oceanography,* 22(1), pp. 84-91, doi: 10.4319/lo.1977.22.1.0084.

Uncles, R. J. & Stephens, J. A., 1990. Computed and Observed Currents, Elevations, and Salinity in a Branching Estuary. *Estuaries,* 13(2), pp. 133-144, doi: 10.2307/1351582.

Visser, A., 1997. Using random walk models to simulate the vertical distribution of particales in a turbulent water column. *Mar. Eco. Prog. Ser.,* Volume 158, pp. 275-281, doi: 10.3354/meps158275.

Yamazaki, H. & Osborn, T. R., 1993. Direct estimation of heat flux in the seasonal thermocline. *J. Phys. Ocenogr.,* Volume 23, pp. 503-516, doi: 10.1175/1520-0485(1993)023<0503:DEOHFI>2.0.CO;2.